Wide-band continuous-wave terahertz source with a vertically integrated photomixer

E. Peytavit, J-F. Lampin, F. Hindle, C. Yang, and G. Mouret

Citation: Appl. Phys. Lett. **95**, 161102 (2009); doi: 10.1063/1.3251071
View online: http://dx.doi.org/10.1063/1.3251071
View Table of Contents: http://apl.aip.org/resource/1/APPLAB/v95/i16
Published by the American Institute of Physics.

Wide-band continuous-wave terahertz source with a vertically integrated photomixer

E. Peytavit,[1,a)] J-F. Lampin,[1] F. Hindle,[2] C. Yang,[2] and G. Mouret[2]
[1]*Institut d'Electronique de Microélectronique et de Nanotechnologie, UMR CNRS 8520, Université de Lille1, Avenue Poincaré, B.P. 60069, 59652 Villeneuve d'Ascq Cedex, France*
[2]*Laboratoire de Physico Chimie de l'Atmosphère, UMR CNRS 8101, Université du Littoral Côte d'Opale, 145 Avenue Maurice Schumann, 59140 Dunkerque, France*

(Received 10 September 2009; accepted 29 September 2009; published online 20 October 2009)

A transverse electromagnetic horn antenna is monolithically integrated with a low temperature grown GaAs vertical photodetector on a silicon substrate forming a vertically integrated photomixer. Continuous-wave terahertz radiation is generated at frequencies up to 3.5 THz with a power level reaching 20 nW around 3 THz. Microwave and material concepts allow both qualitative and quantitative explanations of the experimental results. The thin film microstrip line topology has been adapted for active devices by an Au–Au thermocompression layer transfer technique and seems to be a promising generic tool for a new generation of efficient terahertz devices. © *2009 American Institute of Physics*. [doi:10.1063/1.3251071]

Powerful room-temperature solid-state sources at terahertz frequencies are needed for promising applications such as spectroscopy, imagery, and telecommunications. In particular, tuneable continuous-wave sources with high spectral purity are ideal for gas spectroscopy.[1,2] Since the initial experiments of Brown *et al.*,[3] many researchers have reported generation of continuous-wave terahertz by mixing two infrared laser beams on an ultrafast photodetector lying at the feedpoint of a terahertz antenna[4–7] forming a so-called "photomixer." The photomixer proposed in the first attempt was a low temperature grown GaAs (LT-GaAs) planar photodetector loaded by a silicon-lens coupled spiral antenna (PSA). Up to now, the PSA has been the best device for frequencies in excess of 1 THz. This is in most part explained by the low electrical capacitance of the photodetector ($C \approx 0.5$ fF) which shifts the cut off frequency (f_{RC}) related to the RC time constant well beyond 1 THz. A vertical photodetector integrated to a spiral antenna[6] has been proposed and tested, yielding more terahertz power than PSA up to 900 GHz but less beyond[2] due to its higher electrical capacitance. More recently, we have designed a new terahertz antenna: the transverse electromagnetic horn antenna (TEM-HA).[8] This 3D structure was developed for terahertz pulses emission and characterized in a time-domain configuration. The results show that it is a nondispersive, large bandwidth antenna. Then, the TEM-HA has been monolithically integrated with a planar interdigitated LT-GaAs photoconductor for frequency-domain photomixing.[10] The device provided promising results, but the frequency dependence of the emitted terahertz power was principally governed by electromagnetic propagation effects, such as coupling between photodetector and antenna, and was only weakly dependent of the RC time constant. Furthermore, it became clear that planar photodetectors, waveguides, or antennas on high dielectric permittivity substrates such as GaAs are not efficient beyond 1 THz,[11] unless their dimensions are smaller than ten micrometers. In order to solve this problem and to improve the photomixer bandwidth, a vertical photodetector was integrated with a TEM-HA using a thin film microstrip configuration, in which the same metallic sheet is both the ground plane of the TEM-HA and the bottom bias electrode of the vertical photodetector. This integration is feasible thanks to the use of an epitaxial layer transfer technique based on wafer level Au–Au thermocompression bonding, which is a more suitable bonding technique as regards thermal and electrical characteristics compared to previous attempts based on a polymer layer.[6] We report in this letter a frequency-domain photomixing experiment with such a vertically integrated photomixer (VIP).

A schematic of the fabricated device is presented in Fig. 1. The photodetector consists of a 2.2-μm-thick LT-GaAs epitaxial layer sandwiched between two metallic bias electrodes. The upper electrode, which defines the photodetector active region, is a 10-nm-thick and 5×5 μm^2 area semitransparent gold pad. The lower electrode is a 40-nm-thick Ti/800-nm-thick Au bilayer and is used as the ground plane of the TEM-HA. The antenna consists of a bilayered 20-nm-thick Ti/3.4-μm-thick Au triangular conductive sheet inclined above the ground plane and supported by a polytetrafluoroethylene cuboid, as shown in Ref. 10. The dimensions of the isosceles triangular sheet (length $=3$ mm, base$=2.6$ mm) have been chosen in order to radiate efficiently from 100 GHz to at least 1 THz.[8] The photodetector is linked to the antenna by a 10×12 μm^2 pad, which constitutes the anchor of the antenna.

The device was fabricated using the following procedure: starting from a 450-μm-thick semi-insulating GaAs substrate, a 0.1-μm-thick GaInP layer was grown by gas-source molecular beam epitaxy followed by a 2-μm-thick

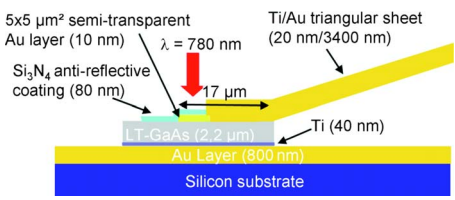

FIG. 1. (Color online) Schematic side-cut of the VIP.

[a)]Electronic mail: emilien.peytavit@iemn.univ-lille1.fr.

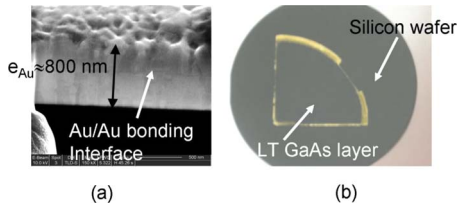

FIG. 2. (Color online) (a) Scanning electron microscope image of a focus ion beam cut of the Au–Au bonding interface and (b) optical view of a LT-GaAs layer reported on a 2-in.-diameter silicon substrate.

layer of low temperature (~200 °C) GaAs. After its growth, the sample was annealed at 580 °C for 1 min. The photocarrier lifetime was measured by time-resolved photoreflectance. The photoreflectivity of the LT-GaAs was found to decrease exponentially with a characteristic time, $\tau_{1/e} \approx 720$ fs. The LT-GaAs epitaxial layer was subsequently transferred onto a 2-in.-diameter *p*-doped silicon wafer. For this purpose, a 40-nm-thick Ti/400-nm-thick Au bilayer was deposited by cathodic sputtering on both the LT-GaAs wafer and the silicon host substrate. Then, the two substrates were aligned face to face and bonded in a commercial bonder (SB6e Suss MicroTec) at 200 °C and under a 2 MPa pressure for 90 min. The very low bonding temperature allows us to hybrid GaAs layers on substrates without matching of their coefficients of thermal expansion. In the present study, we bonded a quarter of a 2-in.-diameter GaAs substrate ($CTE_{300\ K}=5.87\times10^{-6}\ °C^{-1}$) (Ref. 12) on a 2-in.-diameter silicon substrate ($CTE_{300\ K}=2.6\times10^{-6}\ °C^{-1}$),[13] taking advantages of the superior mechanical and thermal properties of the silicon. However, the curvature of the bonded substrates prevents mechanical lapping. The GaAs substrate was therefore removed by means of chemical wet etching in a solution of hydrosulfuric acid and hydrogen peroxide. The high etching selectivity (>1000) between GaAs and GaInP allows us to etch the whole 450-μm-thick substrate. The GaInP etch stop layer is then removed in hydrochloric acid. After removing the GaAs substrate, the high thickness difference between the 2-μm-thick LT-GaAs layer and the 300-μm-thick host silicon substrate flattens the bend. During the process optimization, in order to check the bonding quality and the absence of voids, the LT-GaAs layer was also etched leaving only the two bonded gold layers on the silicon host substrate. Figure 2(a) shows a scanning electron microscope image of a focus ion beam cut through the Au–Au interface. It clearly shows that there are no voids at least at the scale of 100 nm. The bonding interface seems to be similar to gold grain boundaries.

An optical view of a LT-GaAs layer transferred on a silicon wafer is shown in Fig. 2(b). Note that the entire area of the bonded piece is usable for the subsequent technological steps. The $5\times5\ \mu m^2$ 10-nm-thick semitransparent gold pad is then patterned by means of electron-beam evaporation, electron-beam lithography, and lift-off techniques. Then, the LT-GaAs active area is formed by inductive coupled plasma etching with an etch mask defined by electron-beam lithography. A 100-nm-thick silicon nitride layer is added as antireflection and surface passivation coating. The TEM-HA is then fabricated following the procedure given in Ref. 10. A scanning electron beam image of the photomixer is shown Fig. 3.

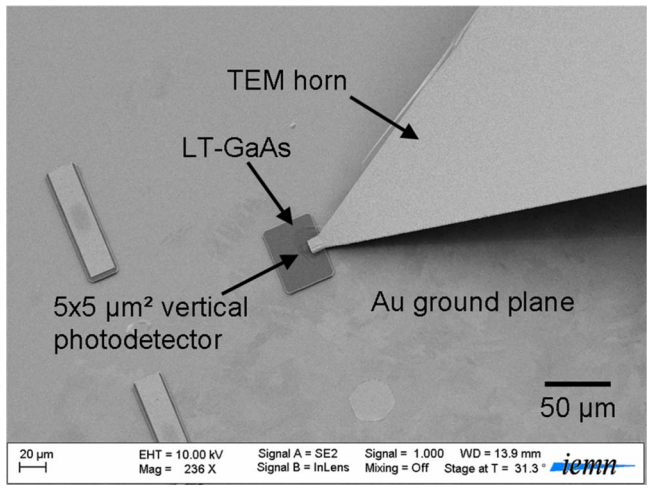

FIG. 3. (Color online) Scanning electron microscope image of the VIP.

The photomixing experimental configuration can also be found in the same letter. The terahertz beam was directly emitted in free space without the need of a silicon lens and was collected by an off axis parabolic mirror and detected by a liquid-helium-cooled silicon bolometer. The detected power was recorded as function of the frequency for a dc photocurrent $i_{dc}=1.76$ mA and is shown in Fig. 4. The absolute terahertz power is estimated assuming a bolometer responsivity of 12 kV/W, given by the manufacturer and obtained from a calibration at 275 GHz using a black-body source and a band-pass filter. In the lowest part of the frequency range, the detected power displays a −10 dB/octave slope as the frequency is increased. The slope become shallower at 2 THz and is nearly flat between 2 and 3 THz. A terahertz power of 20 nW was measured at 2.85 GHz which is to our knowledge the highest output power for a room-temperature wide-band photomixer.[14] In order to understand this frequency dependence of the emitted terahertz power, the VIP photomixer was modeled. The photoconductance *G* of the photodetector is extremely low (typically, $G<0.1$ mS), so we can model the photomixer as a perfect current source in parallel with capacitance and loaded by an antenna[3,14] whose impedance is real ($R_A=65\ \Omega$) (Ref. 9), as shown in the inset of Fig. 4. The $12\times10\ \mu m^2$ anchor of the TEM-HA is modeled as a short thin film microstrip line

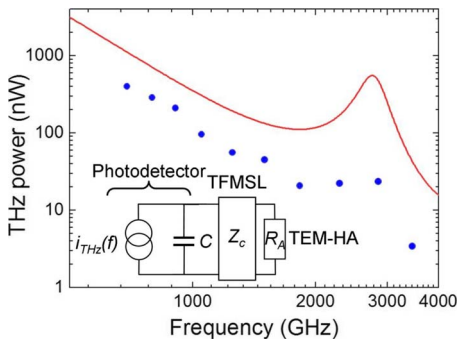

FIG. 4. (Color online) Experimental (circles) and theoretical (solid line) terahertz power emitted by the VIP as function of the frequency. We calculated the terahertz power using the equivalent circuit shown in the inset neglecting losses. Experimental data are obtained with a 12 V bias voltage and 200 mW of optical power at 780 nm. With our 15-μm-diameter optical spot size, we calculated that the effective input optical power on the photodetector is around 50 mW.

(TFMSL) which links the photodetector to the antenna. The capacitance ($C=1.3$ fF) has been calculated in considering that the photodetector is a parallel plate capacitance, with 25 μm^2 area electrodes separated by a 2.2-μm-thick GaAs layer. A 3D electromagnetic simulation was performed on the TFMSL, neglecting dielectric and metallic losses, which showed that the quasi-TEM microstrip mode for a 10-μm-wide and 2.2-μm-thick GaAs TFMSL displays a low dispersion over the entire frequency range. The effective index defined by $n_{\text{eff}}=c_0/v_\varphi$ where v_φ is the phase velocity of the guided wave and c_0 is the vacuum light velocity increases slightly from $n_{\text{eff}}=3.2$ at 200 GHz to 3.4 at 4 THz. Its characteristic impedance (Z_c) varies slightly between 15 Ω at 200 GHz and 18 Ω at 4 THz. In the following study, they will both be considered constant over the entire frequency range and equal to their mean values, i.e., $n_{\text{eff}}=3.3$ and $Z_c=16.5$ Ω. The Schnieder and Heinrich formulas[15] predict, neglecting the thin titanium layer, that the metallic losses reach about 20 dB/mm at 3 THz, and are also negligible for a 12-μm-long TFMSL. Such a thin film microstrip structure is well adapted to very wide bandwidth photomixer. However, this short waveguide has a strong influence on the emitted power. In the present study, the antenna resistance is seen by the photodetector as an impedance Z_s, which is a function of the frequency because of the TFMSL (length=L_g). This is a well known effect in microwave circuits and Z_s can easily be calculated. Neglecting the losses, the real part of Z_s decreases from $R_A=65$ Ω to $R_{\min}=Z_c^2/R_A\approx 4$ Ω at $f_{\lambda/4}\approx 1.5$ THz when $\lambda_0/4n_{\text{eff}}=L_g$. The TFMSL behaves as a so-called quarter-wave transformer. At $f_{\lambda/2}=2f_{\lambda/4}\approx 3$ THz when $\lambda_0/2n_{\text{eff}}=L_g$, Z_s becomes equal to R_A. Furthermore, between $f_{\lambda/2}$ and $f_{\lambda/4}$, Z_s has an inductive component which partially cancels the parasitic capacitance which is no longer negligible between 2 and 3 THz. From the equivalent circuit shown in the inset of Fig. 4, the emitted terahertz power (P_{THz}) can be evaluated as follows: $P_{\text{THz}}=1/2\times R_t\times|i_{\text{THz}}|^2$, with R_t the real part of Z_s in parallel with the capacitance C and $i_{\text{THz}}=i_{\text{dc}}/[1+(f/f_{\tau e})^2]^{1/2}$ to take account of the charge carrier response time.[14] The above expression has been added to Fig. 4 with $i_{\text{dc}}=1.76$ mA, $f_{\tau e}=220$ GHz, $L_g=14.5$ μm, and $C=1.3$ fF. The length of 14.5 μm is used because the current source is considered to be in the center of the photodetector area.

The good qualitative agreement between the experimental and theoretical results can be noted with both exhibiting a -10 dB/octave around 1 THz which decreases as 2 THz is approached. However, there is a more pronounced resonance in the theoretical curve. This discrepancy can have different causes. First, the antenna is assumed to be lossless and to have an impedance real constant and equal to R_A up to 3 THz. It has been experimentally proven up to 1 THz.[8] At higher frequencies, there can be parasitic effects and losses which can attenuate the emitted power. Then, the TFMSL losses could be higher than assumed. Quantitatively, the calculated and experimental results differ only by a factor 2 around 1 THz and 10 at the 2.8 THz resonance which is remarkable for such a free space terahertz experiments.

In conclusion, promising results were achieved with a vertically integrated TEM-HA photomixer. We measured record terahertz power around 3 THz without losing efficiency in the remaining frequency range in comparison with other wideband photomixers and without the need for a silicon lens. The TFMSL structure is well adapted to the terahertz frequency in comparison to a planar structure and can be seen as a generic tool for photomixer or other terahertz active devices. A promising idea is to realize an efficient quarter-wave transformer with a high characteristic impedance in order to improve the matching between the photodetector and the antenna in the 1–3 THz range.

The authors thank C. Coinon, P. Tilmant, and D. Troadec for their technical assistance. This work was supported by the CNRS, the French "Délégation Générale pour l'Armement," and by the "Région Nord Pas de Calais."

[1] A. S. Pine, R. D. Suenram, E. R. Brown, and K. A. McIntosh, J. Mol. Spectrosc. **75**, 37 (1998).
[2] G. Mouret, S. Matton, R. Bocquet, F. Hindle, E. Peytavit, J. F. Lampin, and D. Lippens, Appl. Phys. B: Lasers Opt. **79**, 725 (2004).
[3] E. R. Brown, K. A. McIntosh, K. B. Nichols, and C. L. Dennis, Appl. Phys. Lett. **66**, 285 (1995).
[4] S. Matsuura, G. A. Blake, R. A. Wyss, J. C. Pearson, C. Kadow, A. W. Jackson, and A. C. Gossard, Appl. Phys. Lett. **74**, 2872 (1999).
[5] H. Ito, F. Nakajima, T. Furuta, K. Yoshino, Y. Hirota, and T. Ishibashi, Electron. Lett. **39**, 1828 (2003).
[6] E. Peytavit, S. Arscott, D. Lippens, J. F. Lampin, L. Desplanque, F. Mollot, G. Mouret, S. Matton, P. Masselin, and R. Bocquet, Appl. Phys. Lett. **81**, 1174 (2002).
[7] E. A. Michael, B. Vowinkel, R. Schieder, M. Mickulics, M. Marso, and P. Kordos, Appl. Phys. Lett. **86**, 111120 (2005).
[8] E. Peytavit, J.-F. Lampin, T. Akalin, and L. Desplanque, Electron. Lett. **43**, 73 (2007).
[9] R. T. Lee and G. S. Smith, IEEE Trans. Antennas Propag. **52**, 315 (2004).
[10] E. Peytavit, A. Beck, T. Akalin, J.-F. Lampin, F. Hindle, C. Yang, and G. Mouret, Appl. Phys. Lett. **93**, 111108 (2008).
[11] E. Peytavit, T. Akalin, J.-F. Lampin, F. Hindle, C. Yang, and G. Mouret, 17th International Conference on Terahertz Electronics, Busan, South Korea, 21–25 September 2009 (unpublished).
[12] J. S. Blakemore, J. Appl. Phys. **53**, R123 (1982).
[13] Y. Okada and Y. Tokumaru, J. Appl. Phys. **56**, 314 (1984).
[14] S. M. Duffy, S. Verghese, A. McIntosh, A. Jackson, A. C. Gossard, and S. Matsuura, IEEE Trans. Microwave Theory Tech. **49**, 1032 (2001).
[15] F. Schnieder and W. Heinrich, IEEE Trans. Microwave Theory Tech. **49**, 104 (2001).